Steric Modulation of Electrocatalytic Benzyl Alcohol Oxidation by [Ru(trpy)(R₂dppi)(O)]²⁺ Complexes

Vincent J. Catalano,*,† Ryan A. Heck,† Chad E. Immoos,‡ Anna Öhman,‡ and Michael G. Hill*,‡
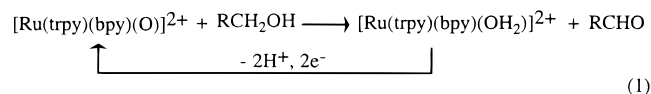
Departments of Chemistry, University of Nevada, Reno, Reno, Nevada 89557,
and Occidental College, Los Angeles, California 90041

The complexes [Ru(trpy)(H₂dppi)Cl]⁺ (**1a**), [Ru(trpy)(Me₂dppi)Cl]⁺ (**1b**), and [Ru(trpy)(Cl₂dppi)Cl]⁺ (**1c**), where trpy is 2,2′,2″-terpyridine, H₂dppi is 3,6-bis(pyrid-2-yl)pyridazine, Me₂dppi is 3,6-bis(6-methylpyrid-2-yl)pyridazine, and Cl₂dppi is 3,6-bis(6-chloropyrid-2-yl)pyridazine, were synthesized and characterized by UV−visible and ¹H NMR spectroscopy. Compounds **1a** and **1b** were additionally characterized by X-ray crystallography. [Ru-(trpy)(H₂dppi)Cl](PF₆)·2CH₃CN crystallizes in the triclinic space group, $P\bar{1}$, with $a = 8.628(1)$ Å, $b = 14.586(2)$ Å, $c = 14.963(2)$ Å, $\alpha = 70.857(8)°$, $\beta = 77.70(1)°$, $\gamma = 74.29(1)°$, $V = 1696.5(4)$ Å³, and $Z = 2$; $R_1 = 0.0739$ ($I > 2\sigma(I)$) with 5920 unique reflections. [Ru(trpy)(Me₂dppi)Cl](PF₆)·0.5(CH₃CH₂)₂O crystallizes in the triclinic space group $P\bar{1}$, with $a = 8.820(2)$ Å, $b = 13.580(2)$ Å, $c = 15.260(2)$ Å, $\alpha = 88.84(1)°$, $\beta = 74.25(1)°$, $\gamma = 73.27(1)°$, $V = 1681.4(5)$ Å³, and $Z = 2$; $R_1 = 0.0693$ ($I > 2\sigma(I)$) with 4407 unique reflections. Reaction of **1a**, **1b**, and **1c** with aqueous silver ion produces the corresponding aqua complexes, **2a**, **2b**, and **2c**, which, after dissolution in acetonitrile, form the analogous acetonitrile complexes, **4a**, **4b**, and **4c**. [Ru(trpy)(H₂dppi)(CH₃CN)](PF₆)(ClO₄)·2 CH₃CN, **4a**, crystallizes in the triclinic space group $P\bar{1}$, with $a = 12.376(1)$ Å, $b = 12.835(2)$ Å, $c = 13.029(2)$ Å, $\alpha = 109.252(9)°$, $\beta = 102.766(8)°$, $\gamma = 90.847(9)°$, $V = 1896.9(3)$ Å³, and $Z = 2$; $R_1 = 0.0397$ ($I > 2\sigma(I)$) with 4844 unique reflections. {[Ru(trpy)(Cl₂dppi)(CH₃CN)](ClO₄)₂}₂·CH₃CN, **4c**, crystallizes in the triclinic space group $P\bar{1}$, with $a = 13.075(2)$ Å, $b = 16.807(3)$ Å, $c = 17.913(2)$ Å, $\alpha = 70.83(1)°$, $\beta = 89.76(1)°$, $\gamma = 82.44(1)°$, $V = 3682.6(1)$ Å³, and $Z = 2$; $R_1 = 0.0777$ ($I > 2\sigma(I)$) with 9459 unique reflections. The redox properties of **1a**, **1b**, **1c**, **2a**, **2b**, and **2c** were examined using cyclic voltammetry and spectroelectrochemistry. In acetonitrile, compounds **1a**, **1b**, and **1c** display reversible 1e⁻ waves assigned to the Ru(III)/Ru(II) couple, while, in aqueous solutions, **2a**, **2b**, and **2c** show pH-dependent, 2e⁻ waves corresponding to the formation of Ruᴵⱽ=O complexes. Second-order rate constants, k_{cat}, for benzyl alcohol oxidation by the Ruᴵⱽ=O complexes were determined electrochemically, yielding values of 22(1) M⁻¹ s⁻¹ for [Ru(trpy)(H₂dppi)(O)]²⁺, 9(3) M⁻¹ s⁻¹ for [Ru(trpy)(Me₂dppi)(O)]²⁺, and 6(4) M⁻¹ s⁻¹ for [Ru(trpy)(Cl₂dppi)(O)]²⁺. Interestingly, the Ruᴵⱽ=O complex with the highest reduction potential ([Ru(trpy)(Cl₂dppi)(O)]²⁺) is the slowest catalyst for benzyl alcohol oxidation. The unusual driving-force dependence of the oxidation rates exhibited by these complexes can be attributed to steric effects that result from incorporating chloro or methyl groups into the 6- and 6′-positions of the dppi ligand. These data are consistent with a mechanism in which the rate-determining step involves preassociation of the substrate with the Ruᴵⱽ=O unit.

Introduction

High-valent ruthenium oxo complexes have been extensively investigated because of their ability to act as catalysts for the oxidation of a wide variety of substrates, including aromatic hydrocarbons, olefins, alcohols, and aldehydes (eq 1).[1] The two

$$[\text{Ru(trpy)(bpy)(O)}]^{2+} + \text{RCH}_2\text{OH} \longrightarrow [\text{Ru(trpy)(bpy)(OH}_2)]^{2+} + \text{RCHO}$$
$$\underset{-2\text{H}^+,\ 2e^-}{\big\uparrow\rule[0.5ex]{8em}{0.4pt}\big\rfloor} \tag{1}$$

most widely studied species are [Ru(trpy)(bpy)(O)]²⁺, and [Ru(bpy)₂(py)(O)]²⁺, where trpy is 2,2′,2″-terpyridine, bpy is 2,2′-

bipyridine, and py is pyridine. Derived from easily synthesized and modified, robust precursors, these complexes provide an ideal opportunity to systematically investigate the subtle mechanistic details of alcohol oxidation.

Previous work has shown that the catalytic rates of oxidation vary tremendously and depend on many factors. For example the second-order rate constant, k_{cat}, for the oxidation of propan-2-ol to acetone by [Ru(trpy)(bpy)(O)]²⁺ in water (6.7 × 10⁻² M⁻¹ s⁻¹) is an order of magnitude larger than that for [Ru(bpy)₂(py)(O)]²⁺ measured in acetonitrile (8.7 × 10⁻³ M⁻¹ s⁻¹).[2]

Electronic effects on the rate of oxidation have also been investigated, as modification to the periphery of the coordinated ligands can alter the Ruᴵⱽ/Ruᴵᴵ couple by as much as several hundred millivolts.[3] Interestingly, there appear to be no simple correlations between the redox couple of the catalyst and rate of oxidation. For example [Ru(trpy)(bpy)(O)]²⁺ and [Ru(trpy)-

† University of Nevada.
‡ Occidental College.
(1) (a) Holm, R. H. *Chem. Rev.* **1987**, *87*, 1401. (b) Meyer, T. J. *J. Electrochem. Soc.* **1984**, *131*, 221C. (c) Madurro, J. M.; Chiericato, G., Jr.; De Giovani, W. F.; Romero, J. R. *Tetrahedron Lett.* **1988**, *29*, 765. (d) Thompson, M. S.; De Giovani, W. F.; Moyer, B. A.; Meyer, T. J. *J. Org. Chem.* **1984**, *49*, 4972.

(2) Thompson, M. S.; Meyer, T. J. *J. Am. Chem. Soc.* **1982**, *104*, 4106.
(3) Lever, A. B. P. *Inorg. Chem.* **1990**, *29*, 1271.

(phen)(O)]$^{2+}$ (phen is 1,10-phenanthroline) have similar redox couples and benzyl alcohol oxidation rates ($k_{cat} \sim 30$ M^{-1} s^{-1}), yet [Ru(trpy)(bpz)(O)]$^{2+}$ (bpz is 2,2′-bipyrazine), which has a higher driving force by 200 mV, exhibits a slower catalytic rate ($k_{cat} = 23$ M^{-1} s^{-1}).[4] However, since these studies were carried out under different conditions, it is not clear whether driving force is the only variable. Roeker and Meyer[5] thoroughly investigated the effect of substrate driving force and found almost no difference in oxidation rates for substituted benzyl alcohol derivatives using [Ru(bpy)$_2$(py)(O)]$^{2+}$ as the catalyst. In contrast, a linear relationship between the driving force and oxidation rates for similarly substituted benzyl alcohol derivatives was found for a loosely related [Ru^{VI}L(O)$_2$]$^{2+}$ complex (where L is a tetradentate macrocyclic ligand).[6]

The mechanism of oxidation has been studied in detail[7] and can proceed via several pathways depending on substrate, catalyst, and conditions. Both one- and two-electron pathways have been considered for the oxidation of alcohols. In aqueous solution, the oxidation is generally believed to occur by the 2e$^-$ route, with hydride transfer comprising the rate-determining step (based on large kinetic isotope effects associated with this process). Under certain conditions, catalyst stability can also become an issue.[8] For example, the Ru^{IV} species can undergo a comproportionation reaction with its corresponding Ru(II) species to form 2 equiv of the Ru(III) complex, greatly complicating mechanistic studies.

The unusual rate behavior may be attributed to the necessity of alcohol−complex association prior to oxidation as suggested by Meyer.[1b] Recent theoretical calculations[9] also support this notion and present a case for alcohol oxygen coordination. In this work, we present the results of a systematic modification of [Ru(trpy)(L)(OH$_2$)]$^{2+}$ (where L = 3,6-bis(pyrid-2-yl)pyridazine (H$_2$dppi), 3,6-bis(6-methylpyrid-2-yl)pyridazine (Me$_2$-dppi), and 3,6-bis(6-chloropyrid-2-yl)pyridazine (Cl$_2$dppi)) and its effect on the electrocatalytic rate of benzyl alcohol oxidation.

Experimental Section

Materials. RuCl$_3$·H$_2$O was obtained from Strem Chemical. All other chemicals were obtained from Acros and used without additional purification.

Instrumentation and Measurements. ^{1}H NMR spectra were obtained on a Varian Unity Plus 500 MHz spectrometer, and all spectra were referenced to TMS as an internal standard. UV−vis spectra were recorded using a Perkin-Elmer Lamda 11 spectrometer using Teflon-stoppered quartz cells having a path length of 1 cm.

Electrochemistry. All electrochemical experiments were performed with a Bioanalytical Systems (BAS) model CV50-W electrochemical analyzer. Cyclic voltammetry (CV) and chronocoulometry (CC) were performed at 20 ± 3 °C with a normal three-electrode configuration consisting of a highly polished glassy-carbon working electrode and a AgCl/Ag reference electrode containing 1.0 M KCl. The working compartment of the electrochemical cell was separated from the reference compartment by a modified Luggin capillary. All three compartments contained a 0.1 M solution of supporting electrolyte.

Acetonitrile (Burdick and Jackson) was distilled from P$_2$O$_5$ prior to use. Tetrabutylammonium hexafluorophosphate, TBA$^+$PF$_6^-$ (Southwest Analytical), was used as received. Acetonitrile electrolyte solutions

were prepared and stored over 80−200 mesh activated alumina (Fisher Scientific Co.) and activated 4-Å molecular sieves.

Potentials are reported vs AgCl/Ag and are not corrected for the junction potential. In acetonitrile, the ferrocenium/ferrocene couple has an $E^{\circ\prime}$ of 0.49 V, with $E_{pa} - E_{pc} = 87$ mV; the corresponding aqueous-solution potential is 0.11 V.

Diffusion coefficients for the Ru(II) complexes were measured using both CV and CC. The electrode area was determined by measuring the electrochemistry of ferrocene in acetonitrile solution, using the known value of 2.4×10^{-5} cm^2/s for its diffusion coefficient.[10]

Digital simulations were performed using the commercial Digisim 2.1 software package from BAS.[11]

Spectroelectrochemistry. UV−vis spectroelectrochemistry was performed at an optically transparent thin-layer cell.[12] The working electrode consisted of vapor-deposited platinum on quartz. Substrates were treated with (3-mercaptopropyl)trimethoxysilane prior to deposition.[13] Data were recorded on a Hewlett-Packard UV-8984 diode-array spectrophotometer.

Preparations. Ru(trpy)Cl$_3$,[14] dppi,[15] Me$_2$dppi,[16] and trpy[17] were synthesized according to literature procedures. Cl$_2$dppi was prepared by a modification of the procedure of Butte and Case[15] using 2-chloro-6-cyanopyridine.[18]

[Ru(trpy)(H$_2$dppi)Cl](PF$_6$) (1a). Ru(trpy)Cl$_3$ (0.320 g, 0.728 mmol) and H$_2$dppi (0.170 g, 0.727 mmol) were refluxed with magnetic stirring for 24 h in 60 mL of EtOH/H$_2$O (3/1 v/v) containing LiCl (0.038 g, 0.902 mmol) and *N*-ethylmorpholine (0.17 mL). The solution was then filtered hot through Celite, and the volume was reduced to about 10 mL on a rotary evaporator. The resulting purple precipitate was collected as the chloride salt on a sintered-glass funnel. The hexafluorophosphate salt was obtained by metathesis of the chloride salt with excess ammonium hexafluorophosphate. Yield: 0.092 g, 16.9%. Anal. Calc: C, 46.5; H, 2.8 N; 13.1. Found: C, 46.16; H, 2.73; N, 12.78. UV−vis (CH$_2$Cl$_2$) [λ_{max}/nm (ϵ_{max}/dm^3 mol^{-1} cm^{-1})]: 278 (1.3 × 10^4), 312 (2.4 × 10^4), 438 (3.1 × 10^3), 524 (5.4 × 10^3).

[Ru(trpy)(Me$_2$dppi)Cl](PF$_6$) (1b). 1b was prepared analogously to 1a. Yield: 25.9%. NMR (Me$_2$CO-d_6): δ 9.07 (d, 2H), 8.81 (dd, 2H), 8.69 (m, 2H), 8.57 (m, 2H), 8.31 (m, 1H), 8.07 (m, 3H), 7.99 (dt, 1H), 7.69 (m, 2H), 7.43 (ddd, 1H), 7.33 (m, 2H), 7.22 (d, 1H), 3.62 (s, 3H), 2.48 (s, 3H). Anal. Calc: C, 45.8; H, 3.6; N, 12.1. Found: C, 45.67; H, 3.37; N, 11.87. UV−vis (CH$_2$Cl$_2$) [λ_{max}/nm (ϵ_{max}/dm^3 mol^{-1} cm^{-1})]: 271 (3.1 × 10^4), 281 (3.0 × 10^4), 315 (5.3 × 10^4), 289 (2.3 × 10^4), 388 (3.9 × 10^3), 478 (9.0 × 10^3), 499 (9.6 × 10^3), 522 (9.5 × 10^3).

[Ru(trpy)(Cl$_2$dppi)Cl](PF$_6$) (1c). 1c was prepared analogously to 1a. Yield: 46.7%. NMR (Me$_2$CO-d_6): δ 8.89 (dd, 1H), 8.75 (d, 1H), 8.69 (m, 2H), 8.55 (dm, 2H), 8.43 (t, 1H), 8.33 (t, 1H), 8.26 (td, 2H), 8.18 (dm, 2H), 8.15 (dt, 2H), 7.90 (t, 1H), 7.56 (dd, 1H), 7.46 (ddd, 2H), 7.39 (dd, 1H). Anal. Calc: C, 48.0; H, 2.9 N; 13.5. Found: C, 47.77; H, 3.09; N, 13.73. UV−vis (CH$_2$Cl$_2$) [λ_{max}/nm (ϵ_{max}/dm^3 mol^{-1} cm^{-1})]: 272 (5.3 × 10^4), 281 (3.8 × 10^4), 312 (5.0 × 10^4), 372 (5.3 × 10^3), 396 (3.6 × 10^3), 477 (8.6 × 10^3), 520 (7.6 × 10^3).

[Ru(trpy)(H$_2$dppi)(H$_2$O)](ClO$_4$)$_2$ (2a). A 0.107 g (0.143 mmol) sample of 1a was gently refluxed in 40 mL of 3/1 acetone/water (v/v) with 0.109 g (0.527 mmol) of AgClO$_4$·H$_2$O for 3 h. The solution was then cooled and filtered through Celite. The volume was reduced to about 5 mL on a rotary evaporator, taking care to keep the temperature below 30 °C. The resulting solid was collected on a sintered-glass funnel. Yield: 80%. Anal. Calc: C, 44.3; H, 3.0 N, 12.5. Found:

(4) Gerli, A.; Reedijk, J.; Lakin, M. T.; Spek, A. L. *Inorg. Chem.* **1995**, *34*, 1836.
(5) Roecker, L.; Meyer, T. J. *J. Am. Chem. Soc.* **1987**, *109*, 746.
(6) Che, C.-M.; Tang, W.-T.; Lee, W.-O.; Wong, K.-Y.; Lau, T.-C. *J. Chem. Soc., Dalton Trans.* **1992**, 1551.
(7) Thompson, M. S.; Meyer, T. J. *J. Am. Chem. Soc.* **1982**, *104*, 5070.
(8) Roecker, L.; Kutner, W.; Gilbert, J. A.; Simmons, M.; Murray, R. W.; Meyer, T. J. *Inorg. Chem.* **1985**, *24*, 3784.
(9) Cundari, T. R.; Drago, R. S. *Inorg. Chem.* **1990**, *29*, 3904.

(10) Kuwana, T.; Bublitz, D. E.; Hoh, G. *J. Am. Chem. Soc.* **1960**, *82*, 5811.
(11) Rudolph, M.; Reddy, D. P.; Feldberg, S. W. *Anal. Chem.* **1994**, *66*, 589A.
(12) Bullock, J. P.; Mann, K. R. *Inorg. Chem.* **1989**, *28*, 4006.
(13) Goss, C. A.; Charych, D. H.; Majda, M. *Anal. Chem.* **1991**, *63*, 85.
(14) Sullivan, B. P.; Calvert, J. M.; Meyer, T. J. *Inorg. Chem.* **1980**, *19*, 1404.
(15) Butte, W. A.; Case, F. H. *J. Org. Chem.* **1961**, *26*, 4690.
(16) Ball, P. W.; Blake, A. B. *J. Chem. Soc. A* **1969**, 1415.
(17) Jameson, D. L.; Guise, L. E. *Tetrahedron Lett.* **1991**, *32*, 1999.
(18) Elman, B. *Tetrahedron* **1985**, *41*, 4941.

Table 1. Crystallographic Data for **1a**, **1b**, **4a**, and **4c**

	1a	**1b**	**4a**	**4c**
formula	$C_{33}H_{27}ClF_6N_9PRu$	$C_{32.75}H_{25}ClF_6N_7O_{0.5}PRu$	$C_{35}H_{30}ClF_6N_{10}O_4PRu$	$C_{64}H_{44}Cl_8N_{17}O_{16}Ru_2$
fw	831.13	806.09	936.18	1792.90
a, Å	8.628(1)	8.820(2)	12.376(1)	13.075(2)
b, Å	14.586(2)	13.580(2)	12.835(2)	16.807(3)
c, Å	14.963(2)	15.260(2)	13.029(2)	17.913(2)
α, deg	70.857(8)	88.84(1)	109.252(9)	70.83(1)
β, deg	77.70(1)	74.25(1)	102.766(8)	89.76(1)
γ, deg	74.29(1)	73.27(1)	90.847(9)	82.44(1)
V, Å^3	1696.5(4)	1681.4(5)	1896.9(3)	3682.6(1)
space group	$P\bar{1}$	$P\bar{1}$	$P\bar{1}$	$P\bar{1}$
Z	2	2	2	2
D_{calc}, g/cm^3	1.627	1.592	1.639	1.617
crystal size, mm	$0.05 \times 0.15 \times 0.46$	$0.06 \times 0.46 \times 0.39$	$0.32 \times 0.18 \times 0.26$	$0.34 \times 0.34 \times 0.40$
μ(Mo Kα), mm^{-1}	0.661	0.664	0.610	0.778
λ, Å	0.710 73	0.710 73	0.710 73	0.710 73
temp, K	173	173	173	173
transm factors	0.99−0.75	0.99−0.76	0.43−0.40	0.99−0.77
R_1,[a] wR_2[b] ($I > 2\sigma(I)$)	0.0739, 0.1051	0.0693, 0.1763	0.0397, 0.0979	0.0777, 0.1829

[a] $R_1 = \sum ||F_o| - |F_c||/\sum|F_o|$. [b] w$R_2 = [\sum[w(F_o^2 - F_c^2)^2]/\sum[w(F_o^2)^2]]^{0.5}$.

C, 44.30; H, 2.82; N, 12.14. UV−vis (H$_2$O) [λ_{max}/nm (ϵ_{max}/dm^3 mol^{-1} cm^{-1})]: 307 (4.8 × 10^4), 330 (2.0 × 10^4), 419 (5.9 × 10^3), 491 (9.8 × 10^3).

[Ru(trpy)(Me$_2$dppi)(H$_2$O)](ClO$_4$)$_2$ (2b). This compound was prepared analogously to **2a**. Yield: 77%. NMR (Me$_2$CO-d_6/D$_2$O, 5/1 v/v): δ 8.78 (d, 2H), 8.71 (d, 1H), 8.69 (d, 1H), 8.63 (d, 2H), 8.44 (t, 1H), 8.34 (t, 1H), 8.29 (d, 1H), 8.12 (m, 2H), 8.13 (d, 1H), 8.07 (dt, 2H), 7.71 (t, 1H), 7.48 (ddd, 2H), 7.32 (d, 1H), 7.15 (d, 1H). Anal. Calc: C, 43.8; H, 3.7; N, 11.5. Found: C, 43.66; H, 3.25; N, 11.30. UV−vis (H$_2$O) [λ_{max}/nm (ϵ_{max}/dm^3 mol^{-1} cm^{-1})]: 312 (7.2 × 10^4), 334 (3.1 × 10^4), 422 (9.8 × 10^3), 486 (1.4 × 10^4).

[Ru(trpy)(Cl$_2$dppi)H$_2$O](ClO$_2$)$_2$ (2c). This compound was prepared very cleanly on an ion exchange column in a manner reported elsewhere.[19] For this work, Whatman CM23 cation exchanger was used in the sodium form. The product was eluted from the column using a solution of 80% acetone−20% 1 M NaClO$_4$. Yield: 82%. NMR (Me$_2$CO-d_6/D$_2$O, 5/1 v/v): δ 8.89 (dd, 1H), 8.78 (m, 3H), 8.61 (dd, 2H), 8.47 (t, 2H), 8.33 (dd, 1H), 8.23 (m, 3H), 8.09 (m, 2H), 7.92 (t, 1H), 7.54 (d, 1H), 7.50 (ddd, 2H), 7.31 (dd, 1H). Anal. Calc: C, 40.8; H, 2.5; N, 11.5. Found: C, 40.66; H, 2.58; N, 11.66. UV−vis (H$_2$O) [λ_{max}/nm (ϵ_{max}/dm^3 mol^{-1} cm^{-1})]: 312 (5.3 × 10^4), 334 (2.6 × 10^4), 410 (3.7 × 10^3), 480 (7.4 × 10^3).

X-ray Structure and Solution. Crystals of **1a**, **1b**, **4a**, and **4c** were grown by slow diffusion of diethyl ether through a thin layer of methanol into an acetonitrile solution of the complex. Suitable crystals were coated with light hydrocarbon oil, mounted on a glass fiber, and placed in the −100 °C nitrogen cold stream of a Siemens P4 diffractometer. Unit cell parameters were determined by least-squares analysis of 29 reflections with 4.37° < θ < 12.58° for **1a**, 23 reflections with 4.22° < θ < 12.50° for **1b**, 27 reflections with 5.09° < θ < 12.46° for **4a**, and 22 reflections with 3.95° < θ < 10.23° for **4c**. A total of 7206 reflections were collected in the range 3.5° < 2θ < 50°, yielding 5920 unique reflections (R_{int} = 0.0387) for **1a,** while 5528 reflections were collected with 3.5° < 2θ < 45.0°, yielding 4407 unique reflections (R_{int} = 0.0960) for **1b**. For **4a**, 5645 reflections were collected, generating 4844 unique (R_{int} = 0.0163) reflections with 3.5° < 2θ < 45.0°, while, for **4c**, 10 976 reflections were collected in the same range, producing 9459 (R_{int} = 0.0657) unique data.

The data were corrected for Lorentz and polarization effects. Crystal data are given in Table 1. Scattering factors and corrections for anomalous dispersion were taken from a standard source.[20]

Calculations were performed using the Siemens SHELXTL PLUS, version 5.03, system of programs refining on F^2. The structures were solved by direct methods. Complex **1a** contained two acetonitrile solvate molecules, while **1b** contained half of a diethyl ether positioned

across the inversion center. There was also a considerable amount of positional disorder for the fluorine atoms of the PF$_6^-$ moiety in **1b**. Complex **4a** also contained two acetonitrile solvate molecules and two slightly disordered anions. Three fluorine atoms of the PF$_6^-$ molecule and one oxygen atom of the ClO$_4^-$ molecule were disordered equally over two positions. The structure of **4c** contained two cations, four anions, and one acetonitrile disordered over two sites in the asymmetric unit. Simple models of all of this disorder provided satisfactory refinements. An absorption correction was applied to **1a** using XABS2,[21] while an empirical model derived from ψ scans was used for **4a**. Neither **1b** nor **4c** benefited from absorption corrections, so none were finally applied. Hydrogen atom positions were calculated using a riding model with a C−H distance fixed at 0.96 Å and a thermal parameter 1.2 times that of the host carbon atom. The largest peak in each final difference map corresponded to 0.96 e/Å^3 and was located 1.46 Å from N(2s) in **1a**, 1.355 e/Å^3 and was located 0.612 Å from F(1) in **1b**, 0.605 e/Å^3 and was located 0.962 Å from F(2) in **4a**, and 1.328 e/Å^3 and was located 1.082 Å from C(4s) in **4c**.

Results and Discussion

Synthesis. The ligands dipyridopyridizine (H$_2$dppi) and dimethyldipyridopyridizine (Me$_2$dppi) are known, while dichlorodipyridopyridizine (Cl$_2$dppi) was synthesized by the reaction of hydrazine with 2-chloro-6-cyanopyridine followed by nitric acid oxidation to produce the dichlorotetrazine base. Treatment of this material with acetylene in boiling dimethylformamide (dmf) produced Cl$_2$dppi in fair yield. The reaction of Ru(trpy)-Cl$_3$ with 1 equiv of dppi, Me$_2$dppi, or Cl$_2$dppi under reducing conditions produced predominantly two different products (eq 2) which are geometric isomers of [Ru(trpy)(R$_2$dppi)Cl]$^+$. The major product of this reaction is the isomer in which the chloro ligand is directed away from the center of the R$_2$dppi ligand (denoted as *out*) while the minor product has the chloro ligand directed in toward the center of the R$_2$dppi ligand (denoted as *in*).

This selectivity likely results from a minimization of lone-pair−lone-pair repulsions between the chloride ligands on the [Ru(trpy)Cl$_2$]$^+$ fragment and the imine lone pairs on the R$_2$-dppi ligand during the initial reaction. Directing the chloride atom toward the outer part of the R$_2$dppi would minimize this repulsive interaction. This reaction also produces small amounts of [Ru(trpy)(R$_2$dppi)$_2$]$^{2+}$ and [Ru(R$_2$dppi)$_3$]$^{2+}$. Column chromatography on alumina, eluting with dichloromethane and

(19) Moyer, B. A.; Meyer, T. J. *Inorg. Chem.* **1981**, *20*, 436.
(20) *International Tables for X-ray Crystallography*; Kynoch Press: Birmingham, England, 1974; Vol. 4.
(21) XABS2: Parkin, S. R.; Moezzi, B.; Hope, H. *J. Appl. Crystallogr.* **1995**, *28*, 53.

Table 2. ^{1}H NMR Chemical Shifts of [Ru(trpy)(H$_2$dppi)(L)]$^{n+}$ Complexes

	H$_2$dppi protons									trpy protons						
L	1	2	3	4	5	6	7	8	9	10	11	12	13	14	15	16
Cl(**1a**)^a	10.39	8.21	8.44	8.93	8.79	8.37	7.48	7.81	7.45	8.63	8.36	8.78	8.59	7.88	7.40	8.00
H$_2$O(**2a**)^b	9.75	8.27	8.45	8.89	8.74	8.23	7.35	7.82	7.45	8.56	8.33	8.77	8.58	7.93	7.42	8.03
CH$_3$CN(**4a**)^c	10.06	8.25	8.55	9.03	8.55	8.93	7.40	7.83	7.48	8.64	8.61	8.92	8.71	8.14	7.52	8.06

^{a} In acetone-d_6. ^{b} In acetone-d_6/D$_2$O (5/1 v/v). ^{c} In CD$_3$CN; chemical shifts relative to Me$_4$Si.

$$(2)$$

"in"   "out"

Scheme 1
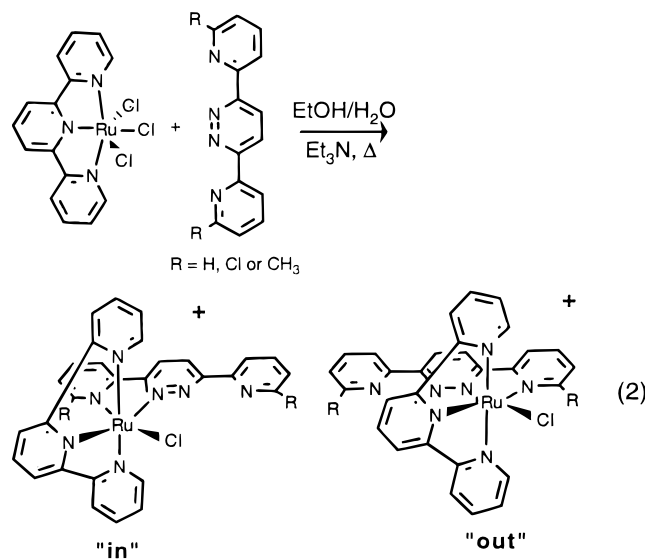
increasing amounts of acetonitrile, effectively separates these species. Often the initial reaction mixture is reduced in volume, causing [Ru(trpy)(R$_2$dppi)Cl]Cl to crystallize out of the solution in analytical purity. It is interesting to note that placing a large, electronegative atom in the 6- and 6′-positions of the dppi ligand still favors the *out* isomer, but by a smaller amount compared to the case of the unsubstituted ligand. This paper discusses only the *out* isomers, and the more elusive *in* isomers will be presented elsewhere.

According to Scheme 1, the chloro species (**1a**, **1b**, **1c**) can be treated with excess AgClO$_4$ in acetone/H$_2$O to produce the corresponding aqua species (**2a**, **2b**, **2c**) in good yield as deep-red, perchlorate salts. The aqua complexes, although highly crystalline, never produced X-ray-quality single crystals. Dissolution in acetonitrile followed by addition of diethyl ether precipitates the acetonitrile species (**4a**, **4b**, **4c**) in a highly crystalline form suitable for X-ray diffraction studies. The Ru^{IV}=O complexes (**3a**, **3b**, **3c**) are generated electrochemically and are not isolated.

The ^{1}H NMR spectra for the complexes further support the formulation and geometry. Chemical shift data are presented in the Experimental Section. Analysis of COSY data, NOE, and selective decoupling experiments provides for complete assignment of all protons of **1a**, **2a**, and **4a** as listed in Table 2. The ^{1}H NMR spectrum of **1a** is presented in the Supporting Information. In acetone-d_6 the dppi proton (H(16) from the X-ray structure) closest to the chloride ligand is shifted significantly downfield to 10.39 ppm due to the large diamag-

netic anisotropy of the chloride ligand, while, in acetonitrile-d_3, it is shifted to 10.37 ppm. The same proton resonance of the acetonitrile complex, **4a**, shifts upfield to 10.06 ppm (CD$_3$-CN) as a result of the larger diamagnetic anisotropy of acetonitrile vs chloride. The corresponding resonance of the aqua complex is shifted upfield to 9.75 ppm. Since the Me$_2$-dppi and Cl$_2$dppi ligands are substituted in this position, no similar downfield resonances are observed for **1b** or **1c**, and the absence of this diagnostic signal prevents the straightforward assignment of all the resonances in these complexes.
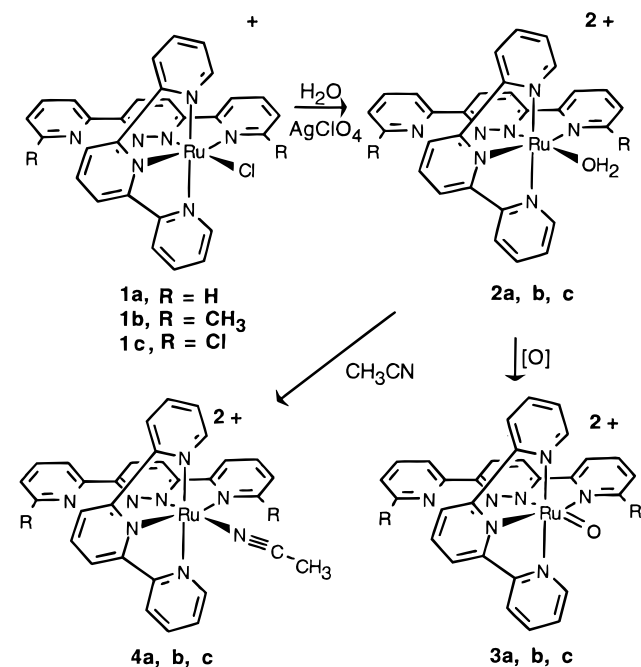
The labile nature of the aqua complexes is demonstrated in the ^{1}H NMR spectra. As expected, the aqua ligands slowly exchange with donor solvents. In acetone-d_6, a second set of nearly identical resonances slowly (1.5 h at 25 °C) appears, assignable to the acetone complex. Addition of a few drops of D$_2$O to the acetone solution eliminates this set of resonances. The more hindered complexes (vide supra), **2b** and **2c**, exchange more slowly, and to a lesser degree.

As expected for low-spin, d^6 Ru(II) ions, these compounds are substitution inert and do not isomerize about the R$_2$dppi ligand. To verify that no isomerization occurs in solution, an acetonitrile sample of **4a** was heated at 70 °C for several hours with no change observed in subsequent ^{1}H NMR spectra. This
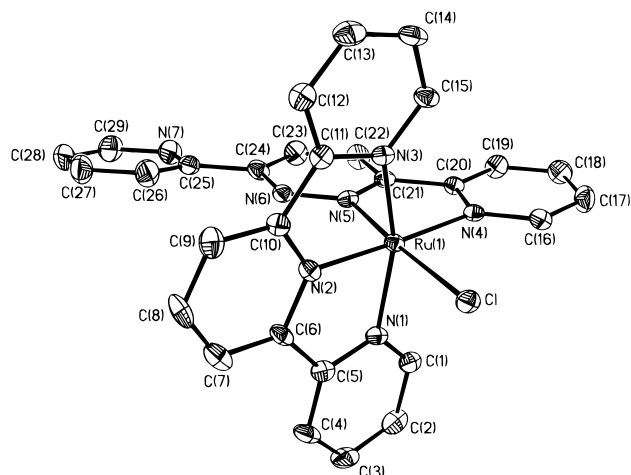
Figure 1. Thermal ellipsoid (40% probability) drawing of [Ru(trpy)-(H$_2$dppi)Cl]$^+$, **1a**, with numbering scheme.

point is reemphasized by the fact that **2a−c** form only as single isomers in good yield.

Electronic Absorption Spectra. The electronic absorption spectra of **1a−c** (CH$_2$Cl$_2$) are typical of [Ru(trpy)(diimine)Cl]$^+$ systems.[6,22] All three complexes have intense $\pi−\pi^*$ absorptions at ca. 272 and 312 nm along with a broad, unsymmetrical band in the visible region of the spectrum assigned to a metal-to-ligand charge transfer (MLCT). The maxima for this MLCT manifold appear at 438 and 524 nm for **1a**, 499 and 522 nm for **1b**, and 477 and 520 nm for **1c**. In pH = 4 phosphate buffer, these MLCT bands shift to higher energy (419 and 491 nm for **2a**, 422 and 486 nm for **2b**, and 410 and 480 nm for **2c**). A similar shift is seen for the acetonitrile complexes as the anionic chloride ligand is exchanged with the neutral acetonitrile molecule. As expected, the more electropositive metal center blue-shifts the λ_{max} of absorption. Further, the low-energy MLCT bands of **2a−c** shift to lower energy (508, 516, and 506 nm, respectively) upon deprotonation (pH = 11) when the coordinated water molecule is exchanged for the weaker-field hydroxide ligand.

Structural Analyses

Structure of [Ru(trpy)(H$_2$dppi)Cl](PF$_6$)·2CH$_3$CN, 1a. The structure of complex **1a** contains the cation, the hexafluoro-phosphate anion, and two acetonitrile solvate molecules. There are no unusual contacts between these moieties. A view of the cation is presented in Figure 1. Selected bond distances and angles are given in Table 3, while atomic coordinates and complete crystallographic details are provided in the Supporting Information. The structure of **1a** shows the Ru atom in a roughly octahedral environment with the trpy ligand coordinated in a meridional fashion. The chloride atom is directed away from the center of the bidentate H$_2$dppi ligand. The pyridine ring containing N(7) is rotated away from the pyridazine ring presumably to remove any steric hindrance between H(26A) and H(24A). These rings are nearly coplanar, with a dihedral angle of 10.2°. The torsion angle defined by N(6)−C(24)−C(25)−N(7) is 170°. Bond distances and angles are typical of Ru(II) polypyridine complexes. Because of the constrained bite of the terpyridine, the Ru(1)−N(2) distance at 1.952(4) Å is shorter than both the Ru(1)−N(1) and Ru(1)−N(3) distances at 2.063(4) and 2.064(4) Å, respectively. Correspondingly, the

(22) Takeuchi, K. J.; Thompson, M. S.; Pipes, D. W.; Meyer, T. J. *Inorg. Chem.* **1984**, *23*, 1845.

Table 3. Selected Bond Distances (Å) and Angles (deg) for **1a**, **1b**, **4a**, and **4c**

Distances				
	1a	**1b**	**4a**	**4c**
Ru(1)−N(1)	2.063(4)	2.061(7)	2.078(4)	2.075(10)
Ru(1)−N(2)	1.952(4)	1.954(7)	1.968(3)	1.969(10)
Ru(1)−N(3)	2.064(4)	2.071(7)	2.071(4)	2.080(11)
Ru(1)−N(4)	2.076(4)	2.154(8)	2.073(4)	2.115(10)
Ru(1)−N(5)	1.996(3)	2.003(7)	2.005(3)	1.986(10)
Ru(1)−Cl	2.4014(12)	2.434(2)		
Ru(1)−N(8)			2.043(4)	2.057(11)

Angles				
	1a	**1b**	**4a**	**4c**
N(1)−Ru(1)−N(3)	159.42(14)	159.1(3)	159.03(14)	159.6(4)
N(1)−Ru(1)−N(2)	79.7(2)	79.8(3)	79.5(2)	80.1(4)
N(2)−Ru(1)−N(3)	79.8(2)	79.6(3)	79.50(14)	79.5(4)
N(2)−Ru(1)−N(4)	175.4(2)	170.1(3)	170.70(14)	169.0(4)
N(2)−Ru(1)−N(5)	96.6(2)	92.4(3)	92.46(14)	91.7(4)
N(4)−Ru(1)−N(5)	78.8(2)	77.6(3)	78.46(14)	78.0(4)
Cl−Ru(1)−N(1)	88.88(10)	87.3(2)		
Cl−Ru(1)−N(2)	88.76(11)	85.2(2)		
Cl−Ru(1)−N(3)	89.09(10)	87.9(2)		
Cl−Ru(1)−N(4)	95.78(10)	104.8(2)		
Cl−Ru(1)−N(5)	174.50(11)	177.5(2)		
N(8)−Ru(1)−N(1)			89.94(14)	84.3(4)
N(8)−Ru(1)−N(2)			93.01(14)	88.4(4)
N(8)−Ru(1)−N(3)			90.66(14)	95.5(4)
N(8)−Ru(1)−N(4)			96.13(14)	101.5(4)
N(8)−Ru(1)−N(5)			174.32(14)	176.1(4)
N(6)−C(24)−C(25)−N(7)	170.0(2)	166.3(3)	179.9(2)	161.9(4)
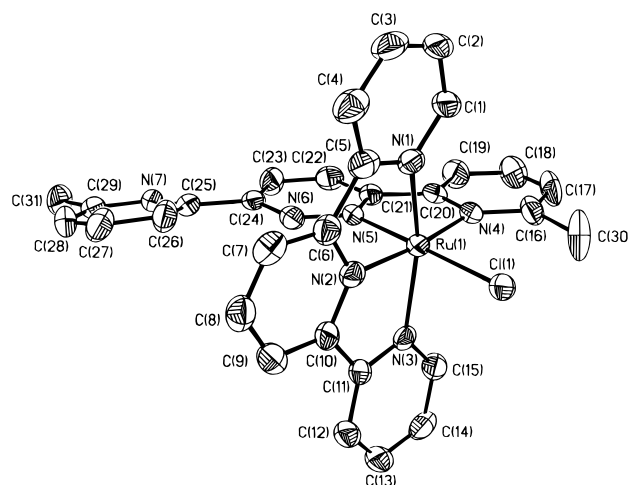
Figure 2. Perspective view (40% probability ellipsoids) of the cation of [Ru(trpy)(Me$_2$dppi)Cl](PF$_6$), **1b**, with numbering scheme.

N(1)−Ru(1)−N(3) bond angle is reduced to 159.42(14)° from the ideal 180°. The H$_2$dppi ligand is bound in a manner similar to that of a bipyridine ligand with Ru(1)−N(4) and Ru(1)−N(5) separations of 2.076(4) and 1.996(3) Å and with N(4)−Ru(1)−N(5) angle of 78.8(2)°. The chloride atom is positioned close to H(16A) with a separation of 2.814 Å, supporting the significant downfield shift observed in the ^{1}H NMR spectrum.

Structure of [Ru(trpy)(Me$_2$dppi)Cl](PF$_6$)·0.5(CH$_3$CH$_2$)$_2$O, 1b. The solid-state structure of **1b** contains the complex, a disordered hexafluorophosphate anion, and half of a diethyl ether solvate molecule with no unusual contacts between any of these species. A drawing of the cation is given in Figure 2, while selected bond distances and angles are given in Table 3. Complete crystallographic data are provided in the Supporting Information.
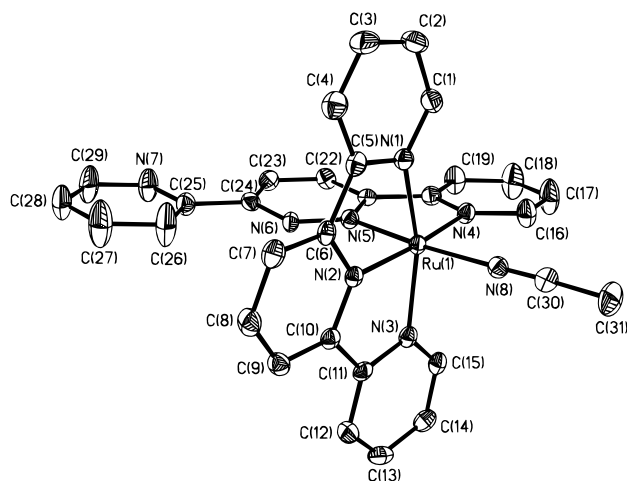
Figure 3. Thermal ellipsoid (40% probability) drawing of [Ru(trpy)-(H₂dppi)(NCCH₃)]²⁺, **4a**, with numbering scheme.

Figure 4. Perspective view (40% probability ellipsoids) of the Ru-(1)-containing cation of [Ru(trpy)(Cl₂dppi)(NCCH₃)]²⁺, **4c**, with numbering scheme.

The structure of **1b** is very similar to that of **1a,** with many similar separations. As seen in **1a**, the pyridine ring containing N(7) is also rotated away from the pyridazine ring with a smaller torsional angle (N(6)−C(24)−C(25)−N(7)) of 166.3°. The most striking difference is seen in an expanded Cl(1)−Ru(1)−N(4) angle of 104.8°. Ideally, this cis angle should be closer to 90°; however, close contact with the methyl group appears to force it away from the Me₂dppi ligand and toward N(2), compressing the Cl(1)−Ru(1)−N(2) angle to only 85.2°. The Ru(1)−Cl(1) bond also lengthens to 2.434(2) in **1b** as a result of this steric crowding. A strong interaction is seen between the methyl protons on C(30) and Cl(1). In the solid state, the Cl(1)−H(30A) separation is only 2.12 Å. This interaction also manifests itself in solution, as evidenced by the large downfield shift for that methyl group compared to the methyl group on the uncoordinated pyridine ring.

Structure of [Ru(trpy)(H₂dppi)(CH₃CN)](PF₆)(ClO₄)·2CH₃CN, 4a. The structure of **4a** contains two acetonitrile solvate molecules along with the cation and two mildly disordered anions. Figure 3 shows a drawing of the cation. The complete crystallographic data are provided as Supporting Information, while selected bond distances and angles are given in Table 3. The structure is very similar to that of **1a** except that the chloride ligand is replaced with an acetonitrile molecule. As seen in Table 3, the Ru(1)−N separations are very similar, including that for the bound acetonitrile with a Ru(1)−N(8) distance of 2.043(4) Å, indicating that it is strongly bonded to the metal center. That there is little change in the angles about Ru(1) in **4a** compared to **1a** suggests that the H₂dppi ligand provides a sterically unencumbered coordination pocket. The N(8)−Ru(1)−N(4) angle of 96.13° is only slightly larger than the related Cl−Ru(1)−N(4) angle of 95.78(10)° in **1a**, and the N(8)−Ru(1)−N(3) angle of 90.66(14)° in **4a** is very close to the ideal cis angle of 90°. Further, the closest contact to H(16A) is N(8), 2.727 Å away. This separation is only slightly closer than that for the corresponding chloride complex **1a**.

Structure of {[Ru(trpy)(Cl₂dppi)(CH₃CN)](ClO₄)₂}₂·CH₃-CN, 4c. The asymmetric unit contains two cations, four perchlorate anions, and two half-occupancy acetonitrile solvate molecules. There are no unusual contacts between these moieties. A drawing of the Ru(1)-containing cation is presented in Figure 4. Both cations are very similar, with one significant difference: the acetonitrile ligand lies on the top side (as viewed in Figure 4) of the Cl₂dppi ligand for the Ru(1)-containing cation, while in the Ru(2)-containing cation it lies below the
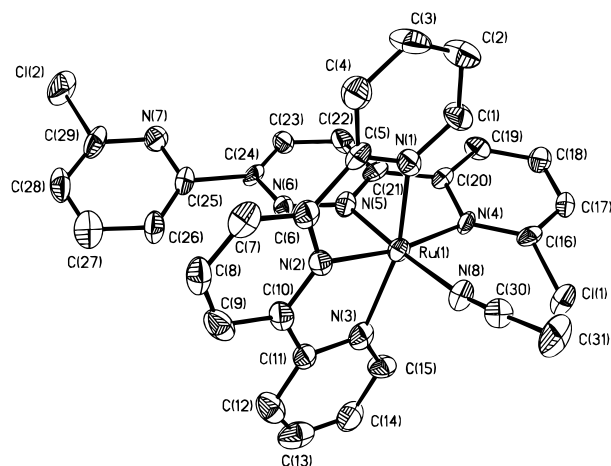
ligand when viewed in a similar orientation. No symmetry elements could be found relating these two cations. A view of the Ru(2)-containing cation is presented in the Supporting Information.

The most striking feature of this complex is the large distortion in the Cl₂dppi ligands caused by interaction with the acetonitrile. Neglecting the uncoordinated pyridine ring of the Cl₂dppi, the average out-of-plane distance for the pyridopyridazine portion of the ligands is 0.12 Å with Cl(1) positioned 0.23 Å below the plane. Despite this large distortion, the Ru-(1)−N separations are very similar to those of **4a**, with a very small elongation observed for the coordinated acetonitrile molecule. The closest nonbonded contact to Cl(1) is N(8), at 3.019 Å. Inspection of the angles around the Ru center better reveals this contortion. The N(8)−Ru(1)−N(4) angle is opened up over 11° to 101.5(4)° as a result of this interaction. The contraction of the N(8)−Ru(1)−N(1) angle to only 84.3(4)° is a result of the acetonitrile ligand being forced up and away from the Cl₂dppi ligands. Selected bond distances and angles are presented in Table 3.

Electrochemistry

In acetonitrile, each [Ru(trpy)(R₂dppi)Cl]⁺ complex undergoes a reversible 1e⁻ oxidation corresponding to the Ru(III/II) couple. Spectroelectrochemical oxidation of [Ru(trpy)(H₂dppi)-Cl]⁺ reveals a strong absorbance at ∼400 nm, in close agreement with the spectra that have been assigned for analogous Ru(III) α-diimine compounds.[17,23] The Ru(III/II) couples span 60 mV, with the Cl₂dppi complex at the most positive value and the Me₂dppi complex at the most negative (Table 4).

In aqueous solution, the analogous aqua complexes undergo a single two-electron oxidation, as confirmed by exhaustive electrolysis (*n* = 2.0 ± 0.3). Figure 5 shows the cyclic voltammogram (inset) of [Ru(trpy)(H₂dppi)(H₂O)]²⁺ in 0.1 M phosphate buffer (pH 7) and illustrates the effect of pH on the redox potential. Between pH 1 and 9, the potential decreases by 60(1) mV/pH unit and then levels off to 30(2) mV/pH unit between pH ∼10.5 and 13. Similar results have been observed for the oxidation of [Ru(trpy)(bpz)(H₂O)]²⁺ [4] and are consistent with a proton-coupled electron transfer shown as follows:

(23) Binstead, R. A.; Stultz, L. K.; Meyer, T. J. *Inorg. Chem.* **1995**, *34*, 546.

Table 4. Electrochemical Half-Wave Potentials (V) and Spectroscopic Data for [Ru(trpy)(R₂dppi)Cl]⁺

	Ru(III/II)[a]	ligand reductions	MLCT λ_{max}, nm (ϵ/M⁻¹ cm⁻¹)[b]
[Ru(trpy)(H₂dppi)Cl]⁺ (**1a**)	0.97	−1.08, −1.44, −1.74	438 (3100), 524 (5400)
[Ru(trpy)(Me₂dppi)Cl]⁺ (**1b**)	0.98	−1.14, −1.39, −1.65	499 (9600), 522 (9500)
[Ru(trpy)(Cl₂dppi)Cl]⁺ (**1c**)	1.04	−0.94, −1.39, −1.57	477 (8600), 520 (7600)

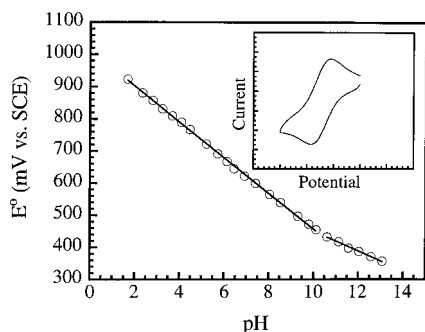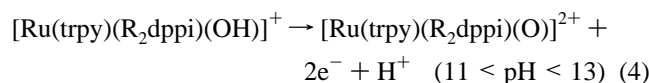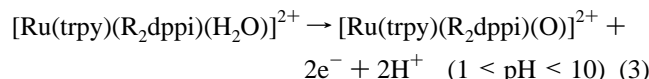[a] Obtained in CH₃CN. [b] Obtained in CH₂Cl₂.

Figure 5. pH dependence of the Ru(IV/II) couple in aqueous solution. Inset: Cyclic voltammogram of [Ru(trpy)(dppi)(H₂O)]²⁺ in 0.1 M phosphate buffer, pH 7 (inset). Scan rate = 100 mV/s.

$$[Ru(trpy)(R_2dppi)(H_2O)]^{2+} \rightarrow [Ru(trpy)(R_2dppi)(O)]^{2+} +$$
$$2e^- + 2H^+ \quad (1 < pH < 10) \quad (3)$$

$$[Ru(trpy)(R_2dppi)(OH)]^+ \rightarrow [Ru(trpy)(R_2dppi)(O)]^{2+} +$$
$$2e^- + H^+ \quad (11 < pH < 13) \quad (4)$$

From the intersection of the low- and high-pH curves, we calculate a pK_a value for [Ru(trpy)(H₂dppi)(H₂O)]²⁺ of 10.3, in excellent agreement with the spectroscopic data. The Me₂-dppi and Cl₂dppi complexes gave similarly well-behaved voltammograms and yielded pK_a values of 10.5 and 10.9. These values were again in good agreement with the spectroscopic data. The lower acidity of the [Ru(Cl₂dppi)(trpy)(OH₂)]²⁺ complex can be rationalized by the weaker σ-donor and stronger π-accepting ability of the Cl₂dppi ligand compared to Me₂- and H₂dppi ligands. Interestingly, the π-acceptor ability of the ancillary ligands appears to be the predominant criterion for determining the relative acidity of the coordinated aqua ligand. This seems to be a general observation for many related [Ru-(trpy)(diimine)(OH₂)]²⁺ complexes.[4,6] Since coordination of Cl₂dppi produces an extremely distorted complex with close ligand contacts, steric encumbrance and hydrogen bonding in [Ru(Cl₂dppi)(trpy)(OH₂)]²⁺ cannot be dismissed. Potentials for the Ru(IV/II) couples of all three complexes are summarized in Table 5.

The appearance of a net two-electron transfer is very unusual for ruthenium α-diimine aqua complexes and implies that the Ru(III) oxidation states of the above complexes are unstable with respect to disproportionation. In a recent study, Meyer[24] compiled an extensive list of Ru(III/II) and Ru(IV/III) couples for similar α-diimine aqua compounds and found that these species generally exhibit sequential one-electron transfers. Interestingly, the thermodynamic stability of Ru(III) was found to correlate with the electronic properties of the α-diimine ligand. In our case, incorporation of nitrogen atoms into the ring system evidently renders the R₂dppi ligands sufficiently poor σ-donors (thereby destabilizing Ru(III))[25] and good π-acceptors (stabilizing Ru(II)) to push the Ru(III/II) couples to

(24) Dovletoglou, A.; Adeyemi, S. A.; Meyer, T. J. *Inorg. Chem.* **1996**, *35*, 4120.
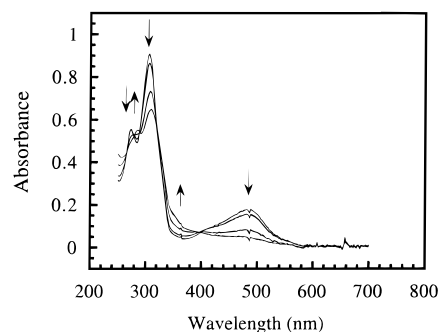

Figure 6. Spectroelectrochemistry of [Ru(trpy)(dppi)(H₂O)]²⁺ in 0.1 M phosphate buffer, pH 7. Spectra were recorded during a slow linear sweep past the Ru(IV/II) couple.
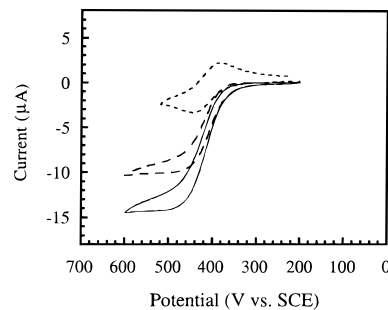

Figure 7. Cyclic voltammogram of [Ru(trpy)(dppi)(OH)]⁺ (pH 11) in the presence of increasing amounts of benzyl alcohol: (---) [BzOH] = 0; (− − −) [BzOH] = 0.048 M; (—) [BzOH] = 0.096 M.

potentials more positive than those of the corresponding Ru-(IV/III) processes.[26]

To quantify the possible role of Ru(III) in the redox chemistry of these R₂dppi species, the aqueous-solution spectroelectro-chemistry (pH 7) of [Ru(trpy)(H₂dppi)(H₂O)]²⁺ was investigated.[27] Figure 6 indicates the clean conversion from Ru^II−H₂O to Ru^IV=O, showing isosbestic points at ∼260, 280, 290, 330, and 390 nm. Significantly, no features due to Ru(III) appear during this experiment; on the basis of the spectrum of Ru(III) in acetonitrile, we conservatively estimate that Ru(III) cannot constitute more than ∼1% of the equilibrium mixture.

Figure 7 shows the effect of benzyl alcohol on the cyclic voltammogram of [Ru(trpy)(H₂dppi)(OH)]⁺ at pH 11. At slow sweep rates (v < ∼20 mV/s) and relatively high concentrations of benzyl alcohol ([BzOH] > ∼0.02 M), the current increases and the $i-V$ curve loses its peak-shape appearance. As reported for similar complexes,[4] these observations are consistent with an electrocatalytic process in which Ru^IV=O (generated at the

(25) The σ-donor ability of the diimine ligand can be correlated to the pK_a of its conguate acid. Introduction of a second nitrogen atom into the ring significantly lowers the pK_a. For example, the pK_a of the conjugate acid of pyrazine is only 0.65, while the pK_a of the conjugate acid of pyridine is 5.2: Perrin, D. D. *Dissociation Constants of Organic Bases in Aqueous Solution*; Butterworth: London, 1965.
(26) Meyer has shown previously[24] that, owing to the proton-coupled nature of the Ru(III)-to-Ru(IV) transformation, the Ru(IV/III) redox couple is much less sensitive to ligand effects.
(27) Hill, M. G.; Mann, K. R. *Inorg. Chem.* **1991**, *30*, 1429.

Table 5. Electrochemical and Spectroscopic Data for Compounds **2a**−**c**

	Ru(IV/II),[a] V	diffusion coeff, cm^2 s^{-1}	k_{cat},[b] M^{-1} s^{-1}	pK_a	MLCT λ_{max}, nm (ϵ, M^{-1} cm^{-1})[c]
[Ru(trpy)(H$_2$dppi)(OH$_2$)]$^{2+}$ (**2a**)	0.385	5.2 × 10^{-6}	22(1)	10.3	419 (5900), 491 (9800)
[Ru(trpy)(Me$_2$dppi)(OH$_2$)]$^{2+}$ (**2b**)	0.365	5.4 × 10^{-6}	9(3)	10.5	422 (9800), 486 (14000)
[Ru(trpy)(Cl$_2$dppi)(OH$_2$)]$^{2+}$ (**2c**)	0.415	4.9 × 10^{-6}	6(4)	10.9	410 (3700), 480 (7400)

[a] Obtained at pH = 11 in aqueous phosphate buffer vs SCE. [b] Second-order rate constant obtained from analytical data as described in text. [c] Obtained in pH = 4 phosphate buffer.

Scheme 2
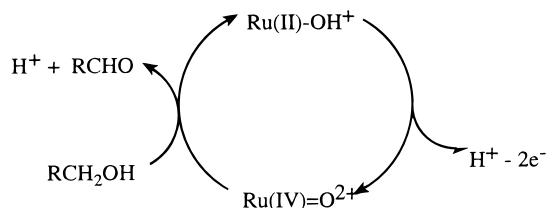
electrode) oxidizes a substrate (benzyl alcohol to benzaldehyde)[1b,28] by 2e$^-$, according to Scheme 2. Under steady-state conditions (in which the Ru^{IV}=O complex is reduced by the alcohol at the same rate it is generated electrochemically), the limiting current is predicted to be independent of scan rate, and the second-order rate constant is given by the expression

$$i_l = nFAC°(Dk_{cat}C_s)^{1/2}$$

(where i_l is the limiting current, n is the number of electrons transferred, A is the electrode area, $C°$ is the concentration of Ru(II), D is the diffusion coefficient, and C_s is the substrate concentration).

In the presence of excess benzyl alcohol, each of the complexes yields scan-rate-independent voltammograms over the limited range 5 < v < 20 mV/s. From a plot of i_l vs [BzOH]$^{1/2}$ for [Ru(trpy)(H$_2$dppi)(OH)]$^+$ (pH 11) a catalytic rate constant, k_{cat}, of 22(1) M^{-1} s^{-1} is calculated. The Me$_2$dppi and Cl$_2$dppi derivatives give similar responses, yielding values for k_{cat} of 9(3) and 6(4) M^{-1} s^{-1} (Table 5). The catalytic rate constants were measured for all three complexes at a minimum of three different [Ru(trpy)(R$_2$dppi)(OH)]$^+$ concentrations, and in each case, the limiting currents varied linearly with initial [Ru(II)].

Catalytic rate constants were also estimated from digital simulations of the voltammetric responses of the various catalysts. For these experiments, four concentrations of benzyl alcohol were used, and the scan rates were varied over a sufficient range to span the steady-state catalytic response to an essentially reversible voltammogram. Representative data for the electrochemistry of [Ru(trpy)(Cl$_2$dppi)(OH)]$^+$ in the presence of 0.10 M benzyl alcohol are included in the Supporting Information. Excellent agreement between the simulated and experimental voltammograms was observed for each scan rate employed. Using this methodology, we calculate k_{cat} values

(28) Kutner, W.; Meyer, T. J.; Murray, R. W. *J. Electroanal. Chem.* **1985**, *195*, 375.

for the dppi, Me$_2$dppi, and Cl$_2$dppi complexes of 24, 6, and 8 M^{-1} s^{-1}, in close accord with the steady-state results.

The data above clearly show that catalyst driving force is not the rate-determining factor for benzyl alcohol oxidation by [Ru(trpy)(R$_2$dppi)(O)]$^{2+}$: [Ru(trpy)(Cl$_2$dppi)(O)]$^{2+}$ has the highest driving force for alcohol oxidation (0.415 V) but shows the slowest catalytic rate (6(4) M^{-1} s^{-1}). In fact, this rate is essentially equal to that of [Ru(trpy)(Me$_2$dppi)(O)]$^{2+}$ (9(3) M^{-1} s^{-1}), which has the lowest driving force of the trio at 0.365 V. The fastest catalyst, [Ru(trpy)(H$_2$dppi)(O)]$^{2+}$, displays an intermediate driving force and has a rate comparable to those of similar catalysts reported elsewhere.[4]

Conclusions

It is clear that incorporating chloro or methyl groups into the 6- and 6′-positions significantly alters the geometry around the Ru center of the catalytic precursors, and although the catalyst structures could not be probed directly by X-ray crystallography, it is likely that the distortions observed for the precursors would be manifested in the electrochemically generated Ru^{IV}=O molecules. Further, the sterically encumbered coordination pocket could hinder the approach of the incoming alcohol molecule and, hence, reduce the rate of oxidation. Our findings demonstrate that the rate of alcohol oxidation does not correlate to the catalyst driving force and further support the notions suggested by Meyer[1b,2,5] that intimate association between the alcohol and the catalyst prior to hydride transfer may be an important factor in the overall rate and that incorporation of a proton acceptor group at an appropriate site structurally may improve catalyst design. With this idea in mind, it may be possible to enhance the overall catalytic rate by rearranging the metal center about the R$_2$dppi ligand ("in" complex from eq 2) to allow the uncoordinated imine groups to act as a proton acceptors. We are actively pursuing this aspect.

Supporting Information Available: An ^{1}H NMR spectrum of **1a**, experimental and simulated cyclic voltammograms recorded under catalytic conditions, and an X-ray structure diagram for the Ru(2)-containing cation of **4c** (4 pages). Four X-ray crystallographic files, in CIF format, are available on the Internet only. Ordering and access information is given on any current masthead page.